



Gaia initial QSO catalogue: the variability and compactness indexes

A.H. Andrei^{1,2,3,4}, S. Anton^{5,6}, C. Barache³, S. Bouquillon³, G. Bourda⁷,
J.-F. Le Campion⁷, P. Charlot⁷, S. Lambert³, J.J. Pereira Osório⁵, J. Souchay³,
F. Taris³, M. Assafin⁴, J.I.B. Camargo¹, D.N. da Silva Neto⁸, and R. Vieira Martins¹

¹ Observatório Nacional/MCT, Rio de Janeiro, Brasil, e-mail: oat1@on.br

² INAF/Osservatorio Astronomico di Torino, Pino Torinese, Italy

³ SYRTE/Observatoire de Paris, Paris, France

⁴ Observatório do Valongo/UFRJ, Rio de Janeiro, Brasil

⁵ Centro de Investigação em Ciências Geo-Espaciais/FCUP, Porto, Portugal

⁶ SIM, Lisbon, Portugal

⁷ Laboratoire d'Astrophysique de Bordeaux, Bordeaux, France

⁸ Universidade Estadual da Zona Oeste, Rio de Janeiro, Brasil

Abstract. The manifold Gaia scientific output rely on precise astrometry accurate to sub-mas standards. This depends on building a fundamental reference frame formed by point-like, position stable, and allsky homogeneous grid points. In one word, quasars. The Gaia CU3 Initial Quasar Catalogue Working Package was established to beforehand produce one such list, although ultimately the satellite multiband photometry aided by astrometric monitoring has the potential to pick up a clean sample of quasars.

Key words. Stars: abundances – AGN: QSO – variability – host galaxy – Gaia

1. Introduction

The Gaia mission will observe solar system, galactic, and extragalactic objects, including about 500,000 QSOs. The satellite observations imply in proper, in the relativistic sense, reference systems to which the measurements are initially referred (Bastian, 2007). The final catalogue will comply to the IAU's sanctioned Barycentric Celestial Reference System (BCRS), resulting in the Gaia Celestial Reference Frame (GCRF) materialized by a dense mesh of fiducial QSOs.

Notwithstanding, it is also worth to mention that two other quite robust extensions of the GCRF will be produced, to brighter regimens. The one formed by the unresolved galaxies (some 10 million of objects) and the QSOs that didn't make it to be in the GCRF (which would presumably contain several radio-loud quasars). And the one formed the approximately half a billion of stars with highly accurate position and proper motions.

QSOs are thus crucial targets to define the GCRF, and accordingly on board means are capable of classifying them. The QSO classification contains three major orientations:

Send offprint requests to: A.H. Andrei

getting the cleanest QSO sample to determine the GCRF; deriving the most complete QSO sample based on the full Gaia data; and determining the astrophysical parameters for each QSO. The determination itself of a Gaia source as a QSO is planned to rely primarily on comparison of the photometric output against a template of spectral energy distributions (SED), and secondarily on astrometric observables, variability analysis and a reliable initial list of known QSOs. The study by (Claeskens et al., 2006) shows that, based on the end-of-mission colour information, supervised Artificial Neural Networks can virtually reject all contaminating stars (including white dwarfs), although the completeness drops to about 20% at G 20th. Notice, however, that a sample as small as 10,000 quasars can stabilize the GCRF to a residual rotation of less than $0.5 \mu\text{as}$ per year, provided they are well distributed over the sky.

The relatively small number of points actually required to constitute a robust GCRF brings particular relevance for an initial list of known QSOs. Which main aim is to obtain a clean sample of at least 10,000 quasars, distributed all sky above -20deg of galactic latitude, with magnitude brighter than $V=20$. This bona fide initial clean sample is useful both for the actual orientation of the GCRF and to enlarge the templates of the recognition scheme. For that, catalogue and published QSO determinations are inspected, amounting to a few thousands. Several criteria were enforced to acknowledge a given source, the most important of which were at least two independent determinations and the existence of spectroscopic redshift.

Presently the GIQC contains 187,505 objects, divided in three categories - defining, candidates, and other. The defining objects are 136,643 well documented QSOs, being 103,422 from the SDSS/DR8 (Schneider et al., 2010). The catalog brings reliable redshift for 183,543 objects (97.87%), and there are reliable optical images for 159,701 objects (85.17%).

The astrometric coordinates of the sources compiled for GIQC are presented in the LQAC2 (Souhay et al., 2011). Their sky den-

sity (4.5 per sq.deg) and sky distribution (about 75% of the minimum distances from adjacent sources are between 1.5deg and 5deg) prompted to combine the set into an optical materialization of the ICRS (Andrei et al., 2009). The distribution is homogeneous, with no empty zones, though there is a quantity decreasing onwards the inner galactic disk, whereas there is an enhancement on the SDSS zones. By comparing with the common ICRF-2 quasars, we find the systematic offsets $\Delta\alpha\cos\delta=+1.6\text{mas}$ ($\sigma=154.9\text{mas}$) and $\Delta\delta=+3.6\text{mas}$ ($\sigma=158.8\text{mas}$). Excluding the optical minus radio residuals deviating by more than 2σ , the adherence to the ICRF2 is obtained as 55.5mas on right ascension and 59.7mas on declination. The zonal warps are mostly (67%) smaller than 50mas, with just 6 zones showing systematics larger than 100mas.

2. Morphology

We derived a PSF-based morphological classification of the GIQC objects using the available the B, R, and I DSS images. The morphological classification derives from comparing the target PSF against the local PSF. To that, neighborhoods of 5×5 arcmin around the QSO are obtained from the DSS plates. From the total LQAC-2 sample were obtained images of 114,606 fields from the B plates, 191,030 fields from the R plates, and 183,421 fields from the I plates. The incompleteness in most cases was due to the sky coverage, and lack of available uncompressed digitalization for the DSS2 blue plates.

The IRAF task DAOFIND is used to detect both stars and target, as well as to derive the PSF parameters. Stars are collected within one magnitude from the QSOs magnitude, but in case less than five stars are picked up the magnitude limits are progressively enlarged at one magnitude steps, except to stars brighter than the tenth magnitude. Stars must be isolated from each other by an inner radius of ten pixels, and within the frame by the same threshold. If less than five comparison stars are found no morphological index is derived for that QSO on that plate. Three estimators of the PSF are used: SHARP (prob-

| RA (deg) | DEC (deg) | MAG | z | Rshr | Rsrn | Rgrn | Bshr | Bsrn | Bgrn | Ishr | Isrn | Igrn | Class |
|----------|------------|-------|-------|------|------|------|------|------|------|------|------|------|-------|
| 0.000000 | -0.032778 | 19.40 | 1.560 | | | | | | | | | | C P |
| 0.002083 | -0.450833 | 20.09 | 0.250 | | | | | | | | | | O F |
| 0.005291 | -2.033269 | 19.29 | 1.356 | 0.75 | 0.10 | 0.13 | | | | | | | D |
| 0.005735 | -30.607458 | 19.18 | 1.143 | 0.20 | 0.01 | 0.91 | | | | | | | D |
| 0.007326 | -31.373790 | 19.74 | 1.331 | 0.73 | 0.44 | 0.00 | | | | 1.82 | 1.14 | 1.37 | D |
| 0.011279 | -25.193609 | 21.56 | 1.314 | | | | | | | | | | O F |
| 0.012178 | -35.059062 | 17.09 | 0.508 | 0.59 | 0.20 | 0.27 | | | | 0.39 | 0.80 | 0.07 | D |
| 0.022792 | -27.419533 | 19.11 | 1.930 | 0.12 | 1.01 | 0.41 | | | | | | | D |
| 0.027500 | 0.515278 | 20.37 | 1.823 | | | | | | | | | | D S |
| 0.033333 | -63.593333 | 17.00 | 0.136 | | | | | | | | | | C A |
| 0.034167 | 0.276389 | 20.03 | 1.837 | | | | | | | | | | D S |
| 0.038604 | 15.298477 | 19.40 | 1.199 | 0.92 | 0.02 | 0.30 | 0.36 | 0.92 | 0.08 | 1.11 | 1.51 | 1.46 | D S |
| 0.039089 | 13.938450 | 18.29 | 2.240 | 0.59 | 0.23 | 0.14 | 0.63 | 0.91 | 0.09 | 2.07 | 0.16 | 1.43 | D S |

Fig. 1. Excerpt from the GIQC (version 3, 2010). The morphological indexes, columns Rshr to Igrn (from the DSS plates B, R, and I) are presented in the text. The first Class column signals the Defining, Candidate or Other classification, while the second one details the classification.

ing skewness), SROUND (probing roundness), and GROUND (probing normalness). Owing to the limited resolution, the morphological indexes are interpreted as presenting the signature of the host galaxy.

To test the power and efficiency of the above procedure applied to the DSS Schmidt plates, a comparative test was made using 1,343 objects present both on the R DSS images and on the r SDSS images (Bouquillon et al., 2010). All nine morphological indexes, namely three parameters in three colors, behaved alike on the DSS and SDSS. Only 1% of the stars were misidentified by the morphological indexes, while for the quasars the correlation between the morphological classification and the SDSS catalogue classification was of 0.86 for the SDSS images and of 0.72 for the DSS images.

The relative distributions of the morphological indexes are shown in the panels of Fig.2. It is evident that the number of non-pointlike QSOs is small but by no means negligible. We found the least of non-pointlike quasars on the B plates and progressively more into the R and I plates, which is expected from the redder emission from the host galaxy than from the inner QSO sources of optical emission.

3. Variability

The intrinsic QSO position stability at the sub-mas level will be over important for the establishment of the GCRF. One should take into account that at the same time that QSOs

are the ideal (or rather the only) choice for fiducial grid points in the establishment of a quasi-inertial celestial reference frame, as prescribed by the ICRS/ICRF paradigm, they are the most energetic and violent, large scale structures in the Universe, active galactic nuclei powered by a super-massive black hole (SMBH). Additionally, the Gaia mission measurements are planned with to an unprecedented precision in photo-center position, which will allow us to investigate the astrometric stability of QSOs and the possible physical consequences. Always according to the standard model of AGNs, a QSO consists of a SMBH (10^6 to 10^{10} solar masses) surrounded by a X-ray and optical continuum emitting region, probably with an accretion disk geometry (see Sulentic et al., 2000), a broad line region (BLR), and a larger region usually referred to as the narrow line region (NLR). These central regions are surrounded by a toroidal structure of dust. The regions emit in different wavelength bands and are supposed to have different dimensions. There are several mechanisms which can cause variation (Andrei et al., 2009): instabilities in the accretion disc around the central black hole: supernova bursts; jet instabilities, and gravitational microlensing. On the other hand, the dusty torus is illuminated from the accretion disk and also re-emits and absorbs, and some variability can be expected in photo-center position due to different illumination of the torus. Recently, (Taris et al., 2011) reported about the magnitude variations of quasars and the potentially correlated motions of their centroids, finding that in one QSO

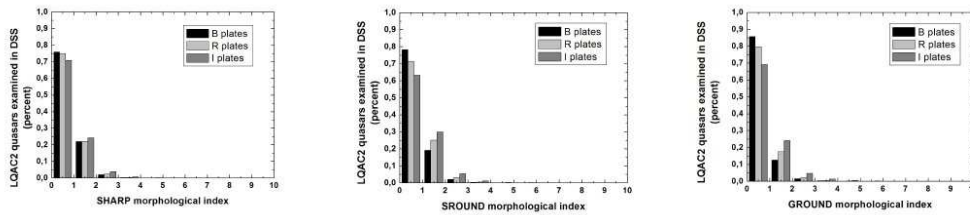


Fig. 2. From left to right the Sharp, Sround, and Ground morphological indexes, for the B, R, I plates from the DSS. Although in all cases most of the QSOs appear as pointlike sources, notice that the fraction of extended sources is non negligible, and the proportion increases from B to I, i.e., from the outshining bluer central central source to the redder host galaxy.

there is a correlation between the centroid motion and magnitude variation.

The variation from the accretion disk emission can be caused by an outburst from the central (compact) continuum source, but also be connected with perturbations in the accretion disk (Jovanovic et al., 2010; Popovic et al., 2011a). In the GIQC the accretion disk and the torus dimensions are being used as variability indexes, in the sense of indicating which objects are apt to suffer a variation on their photocenter along the 5 years of Gaia mission, due to existence of an angularly extended geometry. Popovic et al., (2011b) elaborate this investigation of photocentric variability of quasars caused by changes in their inner structure, We consider perturbations in a relativistic accretion disk; and changes in the pattern of radiation scattered by the dust particles in the surrounding torus, due to the variations in the accretion disk luminosity and dust sublimation radius. As a result it is derived how much these effects may contribute noise, with goal of characterizing any resulting error on the position determination; as well as the estimation of the possibility to observe this effect during Gaia mission, and the group of quasars for which these effects may be dominant.

In principle, to avoid photocenter variation due to perturbations in accretion disk or in the BLR, objects of small dimensions can be chosen for the GCRF. And, to avoid variations of the photocenter due to filaments in the torus, QSOs face on orientated can be chosen. In short, QSOs with high variability are not good objects for construction of the GCRF.

Nonetheless, if the optical variability, that is likely to be sensed by Gaias typical sampling (about 1 month on average), can be linked to the size, if not the preferred direction, of the astrometric jitter, this can be modeled and accounted for. If this is so, the astrometric error budget is alleviated and some variable quasars can be brought back to the GCRF. Conversely, it is important to remark that Gaia astrometric measurements will be very useful for the investigation of the inner quasar structure and physical processes, especially in low redshift variable sources.

Acknowledgements. AHA thanks CNPq grant PQ-307126/2006-0 and the PARSEC International Incoming Fellowship within the Marie Curie 7th European Community Framework Programme.

References

- Andrei, A. H., et al. 2009, A&A, 505, 385
 Andrei, A. H., et al. 2009, Journées 2008
 Bastian, U. 2007, GAIA-CA-SP-ARI-BAS-003-06, Version 6.0
 Bouquillon, S., et al., 2010, Journées 2010
 Claeskens, J. -F. et al., 2006; MNRAS, 367, 879
 Jovanovic, P., et al., 2010, ApJ, 718, 168
 Popovic, L. C., et al., 2011a, A&A accepted
 Popovic, L. C., et al., 2011b, A&A accepted
 Schneider, D. P. et al., 2010; ApJ, 139, 2360.
 Souchay, J., et al., 2011; A&A, accepted
 Souchay, J., et al., 2009; A&A, 494, 799
 Sulentic, J. W., et al., 2000, ARA&A, 38, 521
 Taris, F., et al., 2011, A&A, 526, 25